Material balance and mixing behavior during emulsification of crude oil by using micro-X-ray tomography

*Mostafa Borji, Ahmad Kharrat and Holger Ott**

Department Petroleum Engineering, Montanuniversität Leoben, 8700 Leoben, Austria

Abstract. The emulsification of water and crude oil is typically examined and optimized in test tubes by optical means, i.e., rated outside the porous medium. We examine the rather complex case of crude oil emulsification by alkaline solutions, and follow the question, whether or not those phase behavior experiments are representative for emulsification under the typically laminar flow conditions in porous media. Instead of a qualitative optical evaluation, we use X-ray attenuation coefficients in µCT to establish the material balance during emulsification in the test tubes. We show that in such cases the optical inspection can lead to a considerable misinterpretation of the phase behavior. Using X-ray attenuation makes those experiments quantitative and comparable to µCT-based core flood experiments, where phase mixing occurs in porous media flow. Using X-ray attenuation, we conclusively show that even in the complex case of in-situ saponification by alkaline flooding, (a) emulsification in test tubes and in porous media flow is comparable, and (b) that a minimum emulsion volume with balanced compositions leads to optimal oil recovery in micro-CT-based and conventional core flooding.

1 Introduction

Recovery factors from conventional oil reservoirs using conventional methods reach an average of 35% [1], implying a high remaining potential even after secondary water flooding. Enhanced oil recovery (EOR) methods are developed to target unrecovered trapped and bypassed hydrocarbons and reduce the remaining oil saturation in the reservoirs [2, 3].
Alkaline flooding is one of the economically most attractive chemical EOR methods [4, 5, 6] reported to be an efficient technique for recovering oils containing high amounts of acidic components [7, 8]. In this process, a high pH solution is injected into the reservoir. Upon contact, the alkaline solution undergoes an in-situ saponification reaction with the acidic crude components generating natural surfactants at the oil-water interfaces. These surfactants may lower the interfacial tension (IFT) to a degree that leads to the formation of emulsion phases. By lowering the IFT, capillary trapped oil may be mobilized by substantially increasing the capillary number [3, 9]. Whether the reservoir is a target for alkaline floods or not depends on the total acid number (TAN), which is a measure of the concentration of acidic and thus saponifiable components in the crude oil; the number is defined as the milligrams of potassium hydroxide required to neutralize on gram of crude oil [1]. Candidate fields should have a TAN of 0.5 or higher. [1]. If a high TAN is given, the injection water composition is typically designed by a combination of phase behavior tests and core flood experiments.

The phase behavior is typically tested by bringing crude oil into contact with water of different compositions. The alkali agents, their concentration, and the salinity of the solution are typically varied to optimize the water for injection. Such tests are performed in test tubes and are evaluated visually and qualitatively. This is often sufficient, e.g. for surfactant flooding if the phase behavior is following the Winsor sequence. But this may not be the case for emulsification as result of in-situ saponification of crude. This may have its origin in the wide variety of molecular properties of in-situ surfactants compared to the rather narrow specs of synthetic surfactants in surfactant flooding. It turned out that the interpretation of complex phase behavior may require more sophisticated analytical methods [7, 8]. Even with a quantitative assessment, it may not be easy to find a valid criterion for optimal conditions from phase behavior experiments alone. Then core flood experiment must ultimately lead to the decision.

In this paper, we study the effect of alkaline solutions on emulsification and the displacement of high-TAN crude oil from the Vienna basin. Emulsion formation is evaluated in conventional phase behavior experiments but using the linear mass attenuation coefficient of micro-X-ray computed tomography (µCT) for quantifying the phase compositions and mixing behavior of crude oil and water. The predictive strength and the representativeness of such ex-situ experiments were investigated by the comparison of the results to flooding experiments and imaging emulsion phases under laminar flow conditions. Flooding experiments were performed in µCT-based mini-core floods, and recovery, average phase composition and spatial phase distributions were assessed.

2 Materials and Methods

Fluids: The crude oil sample was derived from the 16 TH reservoir of the Matzen oil field located in Austria. The sample was characterized by viscosity, $\mu = 80$ cP at 20°C, density, $\rho = 0.87$ kg/m^3 at 20°C, and a high total acid number (TAN) between 1.5 [10] and 1.78 mg KOH/g

* Corresponding author: holger.ott@unileoben.ac.at

[11] which makes it a suitable candidate for EOR by alkaline flooding. Detailed field data and the oil composition are reported in several publications [12, 13, 14]. In Order to increase the X-ray contrast to the aqueous phase, 7 wt% Iododecane with 98% purity (Sigma Aldrich) was added; the influence of X-ray doping agents was investigated in a separate study [15] and was minimized.

As injection water, alkaline solutions were prepared by adding sodium carbonate (Na_2CO_3) powder (Sigma Aldrich) as alkali agent in deionized (DI) water, and stirring the solution for ten hours by using a magnetic stirrer. The pH of the solutions was measured using an electronic pH meter and is reported in [7, 16].

Phase Behavior Experiments: Phase behavior tests were carried out by contacting the alkalic solutions with the crude oil in 15 ml glass tubes from Carl ROTH. To minimize any interaction between the fluids prior to the mixing step, we first filled the test tubes with 5 ml of aqueous solution from bottom to top and then added 5 ml of oil. The filling process was done using a high-precision syringe pump (CHEMYX Fusion 200) to guarantee the volumes are equal, and the water-oil ratio is kept at 1. The samples were sealed and then mixed in a rotator (Fisher) for 24 hours at 25 rpm and subsequently put vertically at rest at ambient conditions. To monitor the changes over time, in addition to taking high-quality optical pictures with a NIKON D5600 camera, we performed fast X-ray scans with an in-house µCT scanner (PROCON X-Ray GmbH – CT ALPHA) every 24 hours for three weeks. For the test tube experiments, the scanner was operated at 66 kV and 150 µA with a resolution of 53 µm.

Porous Medium: The flooding experiments were performed in a cylindrical mini-plug with 5 mm diameter and 15 mm length, drilled from a Robuglass® sintered glass filter, representing a 3D porous medium. Such samples were used in earlier studies [17, 18, 19], and are characterized by a high porosity of $\phi = 0.35$ and a high permeability of $K = 22 \pm 2$ D. Pore diameters were reported to be in the range of 40-100 µm, and the total pore volume (PV) was determined to 107 mm^3. This porous medium was chosen for mainly three reasons: (a) the pore space is well resolvable in µCT, (b) it supports laminar flow conditions, and (c), it is made out of borosilicate glass, which is the same material as the test tubes are made of, used for characterizing the phase behavior.

Flooding Experiments: The sample was embedded in a Viton rubber sleeve placed in an X-ray transparent carbon-fiber-epoxy-bases core holder. To mitigate the adverse effects of the rubber sleeve wetting conditions, the sample was wrapped in a single layer of aluminum foil. The core holder was mounted to the sample-manipulation stage of the µCT scanner. High precision VP-series pumps from Vindum Engineering, Inc. were used to inject the fluids and provide the confinement pressure. Three-way high-pressure valves (Swagelok) and PEEK tubes were used as connections and flow lines between the pump, core holder, and the outlet vessel with a sealed cap in which the effluent was collected. For preparation and pre-saturation purposes, a vacuum pump was installed on the downstream side of the flow loop. The oil was then injected under vacuum conditions by means of a Chemyx Fusion 200 syringe pump with a Hamilton gas-tight glass syringe. The experiments were finally carried out in a vertical flooding geometry at ambient pressure and temperature conditions as the phase behavior tests were performed.

3 Quantitative Evaluation of Phase Behavior

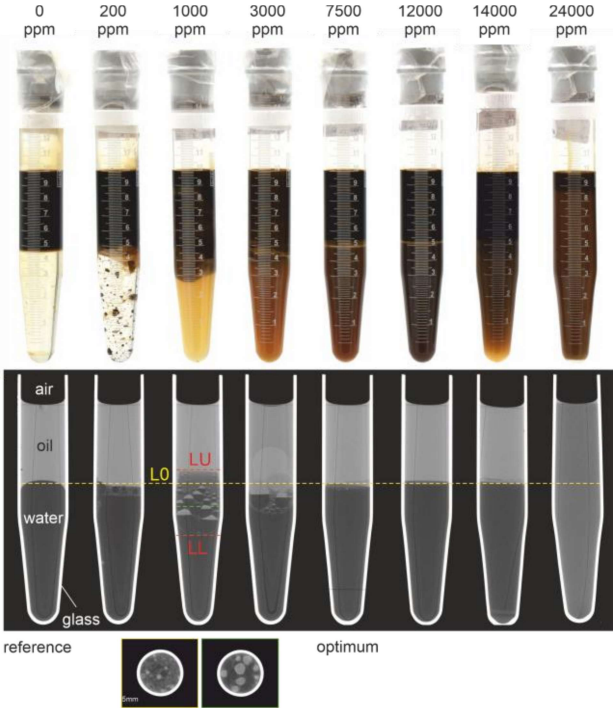

Figure 1: Upper row: optical images of the phase after contacting crude oil with aqueous phases of different Na_2CO_3 concentrations in test tubes. The images are recorded two weeks after mixing at rest. Lower row: µCT scans of the same samples. The yellow line (L0) indicates the oil water contact line of the reference system. For quantitative evaluation, the contact line has been volumetrically corrected for the meniscus. The red lines (upper level LU and lower level LL) represent the extend of the mixing zone as discussed in the text.

To study the type and degree of emulsification, classical phase behavior tests were carried out by contacting the crude oil with aqueous solutions of different Na_2CO_3 concentrations, c_{Na2CO3}. The top row of Figure 1 shows optical images of the phase behavior tests after two weeks of rest. As reported in various studies [20, 21, 11], the mixtures does not follow the conventional Winsor [22] sequence, and a clear trend with c_{Na2CO3} was not observed. At low concentrations (i.e., below 3000 ppm), the aqueous phase is still transparent and optically distinguishable from the swollen oil phase. At higher concentrations, the alkaline solutions become darker and more difficult to differentiate from the oil phase. Above a concentration of 3000 ppm, the phases appear optically mixed indicating strong emulsification. Having a closer

look, a narrow strip of a "third phase" is detectable at 7500 and 12000 ppm c_{Na2CO3}, which disappears at higher concentrations. This phase is rather difficult to be detected by eye, but already indicates, that phases may still be separated despite the homogeneous coloring. But in general, the tests do not give a clear hint, why an optimum displacement efficiency is found at 7500 ppm of Na_2CO_3 [10] – this concentration appears as rather arbitrary with respect to the optically evaluated phase behavior.

Such phase behavior experiments typically ignore that the slightest contamination of water by crude oil may lead to a deep coloring. Therefore, in a next step, we use micro-X-ray tomography for imaging the test tubes. We do this for two reasons: firstly, with the high resolution of the 3D imaging method, we are able to detect interfaces and structures like droplets with sizes above the physical resolution of the image. Secondly, the X-ray absorption contrast directly scales with the fluid density. Therefore, it is possible to quantitatively determine the degree of mixing, which is not possible in the visible spectrum of wavelength.

In the second row of Figure 1, the associated µCT scans are shown. The gray scale directly indicates the density of the fluid phases; the gray values range in between the pure aqueous phase (dark phase, high density) and the pure oil phase (light phase, low density) of the left images (0 ppm), where no mixing is observed and expected – this case is used as reference defining the maximum and minimum gray level. All the other test tubes show a certain degree of mixing, respectively emulsification. The overall result surprises; despite the rather homogeneously appearing coloring in the optical images above 3000 ppm, the X-ray images indicate clearly separated phases up to the 14000-ppm case. Just at the highest concentration, a homogeneous emulsion phase is observed. Furthermore, between 200 and 3000 ppm, heterogeneous phases can be detected in between the aqueous and the oleic phase. The qualitative observations in detail:

- 0 ppm: The meniscus at the oil-water interface indicates that the glass is rather wetted by oil, which is different than what was previously observed for the oil sample of the 8 TH Matzen field [7, 16].
- 200 ppm: A narrow third phase is formed at the oil-water interface, containing dark bubbles of different sizes that may be described as a loose water in oil emulsion.
- 1000 to 3000 ppm: A considerable volume of a third heterogeneous phase is observed at the oil-water contact (OWC). Oil and water bubbles of various sizes (smaller at the top and become larger towards the bottom) were observed.
- 7500 ppm: The oil-water interface becomes flat (no preferential wetting and/or neglectable IFT). A narrow area with a different gray value is observed at the OWC, indicating the formation of a third phase. This middle phase appears as homogeneous.
- 12000 and 14000 ppm: No meniscus at the OWC is observed. The original OWC level is slightly moved upwards indicating swelling of the aqueous phase.
- 24000 ppm: Oil and water seem to be mixed to a high degree forming an isotropic phase similar to a Winsor type IV system. This phase is stable, with no significant changes in time neither optically nor in the X-ray images.

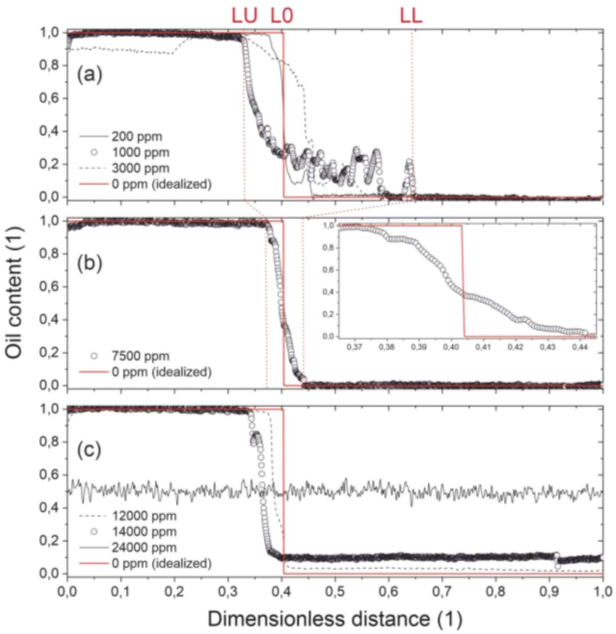

Figure 2 : Oil content as function of distance obtained from the grayscale µCT images as shown in Figure 1. (a) profiles for Na_2CO_3 concentration below, (b) at and (c) above optimum concentration. The data are compared to the reference measurement with 0 ppm Na_2CO_3. The optimum concentration is a result of the present study. The interval LU to LL refers to the mixing zone for selected cases and L0 to the oil-water contact line of the reference case (compare Figure 1).

As already discussed, using X-ray attenuation as analytical method allows a quantitative data interpretation with respect to the material balance. The mixing zone is reflected in the gray scale variation of the resulting phases and the level of the OWC, respectively the boundary levels of an additional occurring phase (UL and LL). Both properties are in the following discussed on basis of vertical density profiles along the central axis of the test tubes as shown in Figure 2.

To make these profiles comparable, the X-ray images were first aligned and the gray values of the fluids averaged over the cross-section. The gray scale was adjusted based on the gray values of glass and air, with X-ray mass-attenuation coefficients that can reliably be considered as constant during the experiment. This led to a consistent scale for all experiments independent of the phase behavior inside the tubes. The gray values of the pure fluid phases were identified from the reference case using deionized water (0 ppm), for which no fluid mixing was observed and expected. Emulsions or in general mixed phases show an intermediate gray value, linearly scaling with the volumetric fluid fractions. This is a result of the volumetric superposition of the mass absorption coefficients in each image voxel. We normalize the gray scale such that the pure oil phase is set to 1 and pure water to 0, directly reflecting the oil content. We ignore the slight variation of the aqueous phase with the alkaline concentration, and we corrected for the slightly varying influence of the test tube material due to its conical shape.

The data are plotted against the dimensionless distance, with 0 being the air-oil contact and 1 the bottom of the test tube.
Changes of the OWC line are described relative to the reference case (L0); the sharp gray value change across the interface (see Figure 1) confirms a good contrast and no detectable mixing of the two fluids. However, the oil-water contact can be misinterpreted due to the interface curvature, which is visible in the X-ray image. The curvature leads to an incorrect interface location in a central line profile, or to an artificial smearing of the interface due to cross-sectional averaging. Therefore, we calculated the volumetric center of the interface, which is given as the red reference level (L0) in the panels of Figure 2. Details on data handling is given in [15].

Concentration dependence: The normalized line profiles for different Na_2CO_3 concentrations in comparison to the base case are shown in Figure 2. Phase (emulsion) boundaries are determined by the first and last points at which the individual profiles deviate from the reference case (0 ppm), given as red lines in panel (a) and (b), for selected cases. The deviation can be with respect to the position of the OWC, or with respect to the gray level of the reference phases. The 200-ppm case shows a rather small deviation from the base case at the interface, essentially indicating the formation of a lower third phase with a low oil content (~ 20%). The profile is as well influenced by a single water bubble in the oil phase. The 1000 ppm profile shows a wide mixing interval with significant fluctuations in the aqueous domain, representing the heterogeneous phase with large oil and water bubbles – a lose emulsion phase; two cross-sections of these structures are shown at the initial OWC and in the lower phase as indicated in the image. At 3000 ppm, even larger scale structures appear. These structures are stable in time, and lead to the rather odd profile in Figure 2 (a).
At 7500 ppm, the total emulsion is significantly smaller in volume than in the aforementioned cases, and the phases become smooth without macroscopic bubbles. Optically, the emulsion phase appears as a narrow stripe at the oil-water contact at the exact height of the volumetrically corrected interface of the reference system, which is comparable to the conventional definition of the optimum condition, a Winsor type III emulsion. Referring to literature and the next section, this system results in the highest recovery factor.
As the Na_2CO_3 concentration increases (12000 and 14000 ppm), the water phase is homogeneously swelling, which is reflected in a rise of the contact line, and in a density decrease, respectively increase of the oil content in the aqueous phase. At even higher alkaline concentrations (above 19000 ppm), the mixing behavior changes significantly. The entire test tube content turns into a stable homogeneous emulsion phase comparable to the Winsor type IV system with an exact average density.

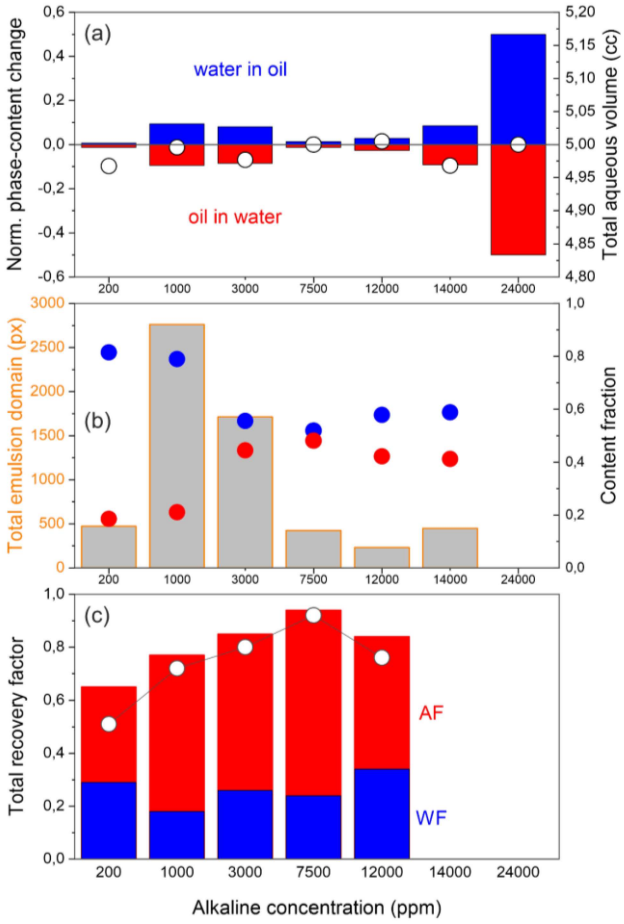

Figure 3 : (a) mutual participating volume of water in oil (blue bars and positive) and oil in water (red bars and negative). The charts are in fraction of the total volume. White circles: the total detected aqueous phase volume in the test tube (initially 5 cc). (b) The total emulsion volume (gray chart bars) and the fraction of water (blue) and oil (red) in the emulsion phase. (c) Recovery factors from the mini-core flood experiments derived from µCT scans. The total recovery factor is split in the contributions of water (blue) and alkaline (red) flooding (cumulative). The incremental tertiary recovery is given by the white circles.

Figure 3 (a) and (b) summarize these results. The data clearly show that at the optimum concentration of 7500 ppm, the mutual solubilization is well balanced and confined to the original OWC. For the other cases, the content fraction – the average fraction of water and oil in the emulsion phase – is rather on the water side, i.e., the emulsion phase is dominated by water.

4 Phase Mixing and Distribution in the Pore Space

The key question to be answered is whether or not the phase behavior in the classical test tube experiments is representative for porous media flow. This is not a trivial question, because the mixing regimes are entirely different; while in porous media flow the flow, respectively mixing regime is laminar, in test tube experiments, mixing is turbulent and the phases are finally observed in equilibrium at rest. To answer this question, we perform mini-core flood experiments including saturation monitoring by in-situ µCT scanning. In all

experiments, secondary water floods at an initial saturation state of $S_o = 1$ were performed, followed by tertiary floods with water of different Na_2CO_3 concentrations. To make the situations comparable, we use the exact same fluids, thermodynamic conditions and solid material (borosilicate) in both type of experiments. We use also the same analytical method – X-ray attenuation – for the evaluation of the resulting phases. However, before we discuss the phase behavior, we discuss the achieved recovery factors in order to identify, respectively verify the optimum alkalinity on basis of the displacement efficiency.

Recovery factor: For calculating the recovery factors, the individual fluid phases were firstly segmented and the volume fractions of oil and water were calculated. We applied two-phase segmentation by thresholding, and therefore, emulsion phases are not explicitly considered. This was not possible for the 24000-ppm case, in which the emulsion phase dominates the end of the tertiary flood. Figure 3 (c) shows the total recovery factor defined as the displaced oil (at initial saturation $S_o = 1$) and split in to the effect of water flooding (blue contribution to the bars) and alkaline flooding (red). The incremental tertiary recovery factor refers to the displaced oil by alkaline flooding with reference to the remaining oil after secondary water flooding. The secondary recovery ranges between 0.18 and 0.34 with an average of 0.26 and a standard deviation of 0.06. The incremental tertiary recovery is with 0.51 lowest at 200 ppm, but monotonically improves with alkaline concentration until reaching its maximum of 0.89 at 7500 ppm. From the recovery factor as well as from the phase behavior, we interpret 7500 ppm as the optimum alkaline concentration, which agrees with earlier conventional core flood experiments [10]. Due to the complexity of the 24000-ppm case, which will be discussed later, the respective recovery results are not included in the diagram.

Average phase saturations: As has been shown in the previous section, the water and oil phases have different X-ray attenuation coefficients and are therefore distinguishable in µCT scanning. This is reflected in the volume-averaged histogram of the µCT scans as shown in Figure 4. The phases are identified by their position on the grayscale axis, while their volumetric contributions (phase saturations) are given by their frequency (the number of µCT voxels in the gray scale interval). Emulsions are mixtures and must appear at intermediate gray values.

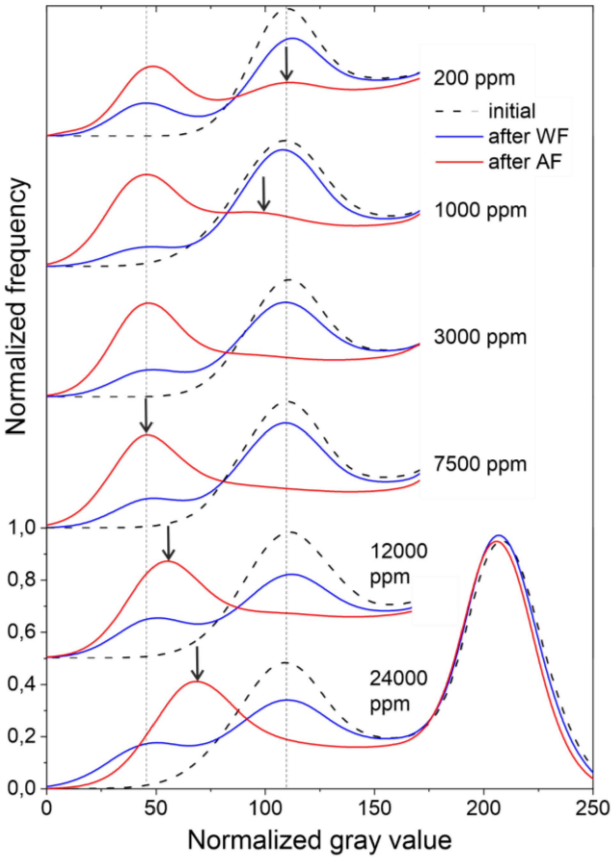

Figure 4 : µCT gray-value histograms of flooding experiments with varying alkaline concentrations. The states before and after water flooding and after the subsequent alkaline floods are shown as black-dashed, blue, and red lines, respectively. The peak on the right correspond to the solid grains; middle peaks represent the crude, and left peaks are related to the water/aqueous phase. Vertical dashed show the original peak positions. The arrows indicate shifts referring to phase mixing.

Figure 4 presents the µCT histograms of the performed flooding experiments. The histograms were taken from the entire scanned field of view, before and after waterflooding and after subsequent alkaline flooding.
The initial-state histograms show a bimodal distribution; the right, dominant peak (at ~210) corresponds to the solid material and the second and weaker peak (at 110~) to the oil phase initially occupying the pore space. The contribution of the solid phase shows a reasonably constant contribution since the solid phase doesn't change throughout the experimental series.
During waterflooding, a fraction of the oil became immiscibly displaced by the injected water. The presence of water in the system was detected by the emergence of a new peak at gray levels lower than that of the doped oil. The water peak intensity is directly proportional to the water saturation and complimentary related to the oil peak intensity. A comparison between the oil peaks before and after the waterflooding shows a decrease in height that indicates oil displacement, and no significant shift in their gray values, pointing out that there is no compositional change of phases during immiscible displacements on a scale smaller than a voxel size.
Subsequent alkaline floods result in further oil displacement, i.e., a further reduction in oil saturation

(except for the 24000-ppm case that will be discussed separately). This is reflected in an increasing water peak on expense of the oil-peak intensity. Contrary to the waterflooding scenarios, oil and water peaks after alkaline flooding show lateral shifts that are attributed to phase density changes caused by solubilization of the respective other fluid phase. An increase in the aqueous-phase oil content (i.e., oil-in-water emulsions) causes the water peak to shift towards higher gray values, and with increasing water content in the oil phase (i.e., water-in-oil emulsions), the oil peak laterally shifts towards lower gray values. The vertical lines in Figure 4 indicates the water and oil peak positions, and the arrows mixing-related shifts. Case-by-case, the following can be stated:

- 200 ppm: There is additional displacement by alkaline flooding, but no significant peak shift is detected, i.e., in the sensitivity of the measurement, there is no emulsion phase forming.
- 1000 and 3000 ppm: There is more additional recovery than in the 200-ppm case as indicated in the peak intensities. A lateral shift in the of the peak positions suggests the formation water-in-oil emulsion. For 3000 ppm, the oil peak nearly disappeared.
- 7500 ppm: The water peak shows no lateral shift, and there is no clearly detectable oil peak since the oil saturation was significantly reduced. Emulsion phases are undetectable.
- 12000 ppm: The aqueous-phase peak shows a slight shift indicating that oil was solubilized in water. The oil peak intensity is strongly reduced, but detectable.
- 24000 ppm: The histogram becomes bimodal after alkaline flooding. The peak position of the left peak shows a maximum at a gray value representing an average phase density in between oil and water. The bimodality suggests a Winsor type IV emulsion system as observed in the test tube experiments. The peak position is more on the water side, which is explained by the already displaced oil volume; there is more water than oil in the system. Interestingly, the emulsion phase remained in the system with a high peak intensity, even after 25 PV of alkaline flooding. It seems that the formed emulsion phase remains stationary in the pore space, without displacement by further alkaline-water injection.

3D phase distributions: More advanced fluid-phase segmentations were performed using *ilastik*, a machine learning image segmentation tool, in order to study the spatial phase distribution, with focus on emulsion phases. Contrary to the water and oil phases, emulsion phases were nor characterized by a dedicated and separable grayscale, but rather appeared as volumes of gradually changing gray levels. Identification and segmentation of emulsion phase were carried out by utilizing histograms and grayscale shifts. For those cases with well separated aqueous- and oil-phase peaks, the images were segmented twice: a) using the water and oil mean values identified from respective waterfloods and b) with respect to the oil-aqueous phase boundary gray level obtained from tertiary floods. The difference of the images using both segmentation methods result in an estimation of the emulsion phase contribution.

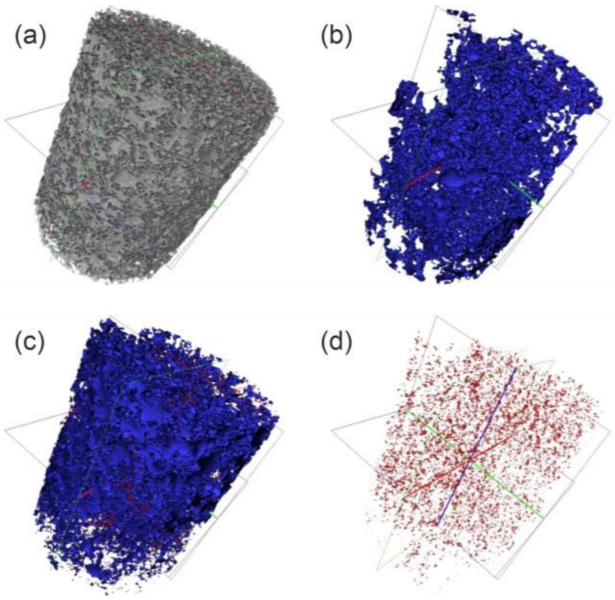

Figure 5 : Three-dimensional visualization of the field of view of the 200-ppm-Na_2CO_3 flooding experiment. (a): pore space, (b): water saturation after water flooding, (c): water saturation and generated emulsion phase (red) after alkaline flooding, and (d): the extracted emulsion phase.

Figure 5 shows the 3-D visualization of the 200-ppm flooding experiment's field of view. The pore space was derived from the initial scans at $S_o = 1$ and is shown in (a). The water-invaded pore space after water flooding is shown in (b). The water saturation of 28% corresponds to the recovery of oil from this volume. Subsequent alkaline injection resulted in a further decrease in oil saturation and in-situ formation of emulsions as shown in (c). In Figure 5 (d), only the emulsion phase is shown, which exists as small isolated clusters spread through the imaged domain.

Figure 6 shows a sub-volume with a detailed phase distribution of the 24000-ppm experiment. The extracted pore space is shown in (a) and (b). The water-phase distribution after secondary water flooding is shown in (c); 36% of the oil was displaced in this process. After alkaline flooding, the histograms indicated a single emulsion phase in the volume without separate aqueous and oil peaks present. After *ilastik* segmentation, we indeed found a dominance of a homogeneous emulsion phase (Figure 6 (d) and (e)). However, also a pure oil phase was detected, with a saturation of 9% and in the form of small clusters (dark gray phase in Figure 6 (f)). No separate aqueous phase was observed, which is quite surprising, because the images were taken under (alkaline) water injection.

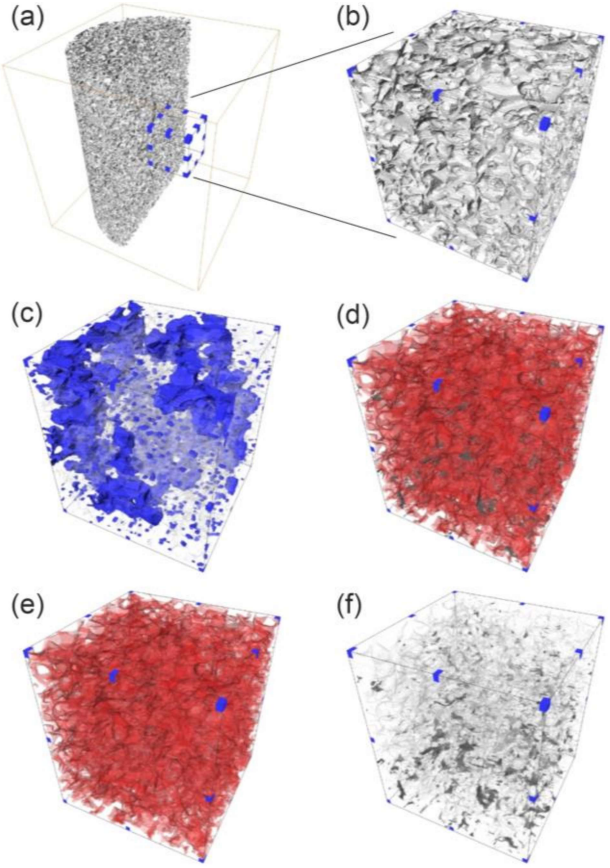

Figure 6 : 24000-ppm flooding experiment: (a) and (b): pore space of extracted sub-volume. (c): immiscible displaced oil (blue) after waterflood. (d): significant emulsion (red) formation and remaining oil (gray) after alkaline flooding. (e) and (f): extracted emulsion phase (red) and remaining oil clusters (gray) after Na_2CO_3 injection.

5 Summary and Conclusions

We investigated the concentration dependence of sodium carbonate on crude oil emulsification. The target scenario is alkaline flooding of a field in the Vienna Basin from which the oil sample was taken. We targeted both, emulsification under turbulent mixing conditions in test tubes and under laminar conditions in porous media flow. We do this in order to investigate whether or not those phase behavior experiments are representative for displacement conditions.

During screening it turned out that the optically evaluated phase behavior was not in alignment with the results of flooding experiments; a complex phase behavior was observed with no link to the optimum sodium carbonate concentrations of 7500 ppm observed in classical core flood experiments and in micro-core flooding, which coincided. The resulting question was about the value of ex-situ phase behavior experiments. This seemed to be a problem especially for alkaline flooding, which is a consequence of the naturally wide variation of the molecular properties of acidic crude components; the resulting variety of generated surfactants may not lead to a Winsor type of phase behavior as expected from synthetic surfactants with rather narrow molecular specifications. The issue of the comparability of experiments was solved in this study by using X-ray µCT to quantitatively analyze both type of experiments. From the present study, we are able to make the following statements:

1. Classical phase behavior tests may be misleading if visually evaluated.
2. An evaluation using X-ray attenuation of fluids by comparison is objective and can be made quantitative in terms of exact phase compositions.
3. Observations under laminar flow conditions in porous media are comparable with the phase behavior tests under rather turbulent mixing conditions in test tubes. Discrepancies between them can be understood in terms of a changing oil-water ratio by the displacement process and the limited spatial resolution of µCT scanning.
4. As for classical surfactant flooding, in alkaline flooding the optimum condition goes along with well-balanced and interface-confined emulsification in test tube experiments. Otherwise it does not follow the classical Winsor picture. The confinement to the interface leads to an undetectable emulsion phase in µCT-based core flooding.

Ongoing investigations – an outlook: As previously shown in 2D microfluidics [7, 16], a statistical analysis of the oil-phase topology delivers robust results on chemical injection-water optimization. With the presented 3D data set and additionally performed 2D-microfluidic experiments on the same fluid system (not presented here), we can show (preliminary data) that the previously found 2D topological fingerprint is reproduced in 3D. Especially Lorenz plots on the cluster-volume statistics are robust indicators for EOR performance. This is far from trivial, since the observed cluster volumes in 3D µCT and 2D microfluidics are quite different on an absolute basis. With the present study, we are certain that the combination of microfluidics and classical phase-behavior experiments with X-ray monitoring provides conclusive results on chemical screening. Both proposed methods can be performed in high throughput and are therefore suitable EOR screening methods.

Acknowledgements

The work has partly been performed in the frame of the EmulPore project funded by The Austrian Research Promotion Agency (FFG), with the OMV Exploration & Production GmbH as project partner. The authors would like to acknowledge Pit Arnold, Rene Ritter for their experimental support, and Dr. Torsten Clemens for valuable discussions.

References

[1] L. W. Lake, Fundamentals of enhanced oil recovery, 2nd ed., Richardson Texas: Society of Petroleum Engineers, 2014.

[2] V. Alvarado and E. Manrique, "Enhanced oil recovery: an update review," *Energies,* 2010.

[3] J. J. Sheng, Modern chemical enhanced oil recovey: theory and practice, Burlington: Elsevier Inc., 2011.

[4] C. E. Cooke, R. E. Williams and P. A. Kolodzie, "Oil recovery by alkaline waterflooding," *Journal of Petroleum Technology,* 1974.

[5] J. J. Sheng, Enhanced oil recovery field case studies, Amsterdam: Gulf Professional Publishing, 2013.

[6] M. Tang, G. Zhang, J. Ge, P. Jiang, Q. Liu, H. Pei and L. Chen, "Investigation into the mechanisms of heavy oil recovery by novel alkaline flooding," *Colloids and Surfaces A: Physicochemical and Engineering Aspects,* 2013.

[7] H. Ott, A. Kharrat, M. Borji and P. Arnold, "Fluid-phase topology of complex displacements in porous media," *Physical Review Research,* 2020.

[8] Y. She, C. Zhang, M. A. Mahardika, A. Patmonoaji, Y. Hu, S. Matsushita and T. Suekane, "Pore-scale study of in-situ surfactant flooding with strong oil emulsification in sandstone based on X-ray microtomography," *Journal of Industrial and Engineering Chemistry,* 2021.

[9] D. W. Green and G. P. Willhite, Enhanced oil recovery, 2nd ed., Society of Petroleum Engineers, 2018.

[10] B. Schumi, T. Clemens, J. Wegner, L. Ganzer, A. Kaiser, R. E. Hincapie and V. Leitenmueller, "Alkali/Cosolvent/Polymer Flooding of High-TAN Oil: Using Phase Experiments, Micromodels, and Corefloods for Injection-Agent Selection," *Society of Petroleum Engineers,* 1 May 2020.

[11] D. Magzymov, T. Clemens, B. Schumi and R. T. Johns, "Experimental Analysis of Alkali-Brine-Alcohol Phase Behavior with High Acid Number Crude Oil," 2020.

[12] S. Poellitzer, M. Gruenwalder, G. Kienberger and T. Clemens, "How to Optimise Oil Recovery after almost 60 Years of Production from the Matzen Field, Austria.," 2008.

[13] M. Lüftenegger, R. Kadnar, C. Puls and T. Clemens, "Operational Challenges and Monitoring of a Polymer Pilot, Matzen Field, Austria," 2015.

[14] B. J. 2. Rupprecht, "Hydrocarbon Generation and Alteration in the Vienna Basin," PhD Thesis, Leoben, 2017.

[15] M. Borji, Phase behavior and pore-scale study of complex alkali-based EOR processes, Leoben: Montanuniversität, 2021.

[16] H. Ott, A. Kharrat, M. Borji, T. Clemens and P. Arnold, "Screening of EOR potential on the pore scale by statistical and topological means," *International Symposium of the Society of Core Analysts,* 2019.

[17] A. Georgiadis, S. Berg, G. Maitland and H. Ott, "Pore-Scale Micro-CT Imaging: Cluster Size Distribution During Drainage and Imbibition," *Energy Procedia,* pp. 521-526, 2012.

[18] A. Georgiadis, S. Berg, A. Makurat, G. Maitland and H. Ott, "Pore-Scale Micro-Computed-Tomography Imaging: Non-Wetting Phase Cluster Size Distribution During Drainage and Imbibition," *Physical Review E,* 2013.

[19] S. Berg, R. Armstrong, H. Ott, A. Georgiadis, S. Klapp, A. Schwing, R. Neiteler, N. Brussee, A. Makurat, L. Leu, F. Enzmann, J. O. Schwarz, M. Wolf, F. Khan, M. Kersten, S. Irvine and M. Stampanoni, "Multiphase Flow in Porous Rock Imaged Under Dynamic Flow Conditions with Fast X-Ray Computed Microtomography," *Petrophysics,* pp. 304-312, 2014.

[20] A. R. Sagi, M. C. Puerto, Y. Bian, M. C. A., H. G. J., M. Salehi and J. T. Kwan, "Laboratory Studies for Surfactant Flood in Low-Temperature, Low-Salinity Fractured Carbonate Reservoir," in *Society of Petroleum Engineers*, 2013.

[21] J. Wegner and L. Ganzer, "Rock-on-a-Chip Devices for High p, T Conditions and Wettability Control for the Screening of EOR Chemicals," in *Society of Petroleum Engineers*, 2017.

[22] P. A. Winsor, "Hydrotropy, solubilization and related emulsification processes," *Transactions of the Faraday Society,* 1948.